ADVANCED MATERIALS TECHNOLOGIES
www.advmattechnol.de

Chalcogenide Glass IR Artificial Compound Eyes Based on Femtosecond Laser Microfabrication

*Shaokun Wang, Fan Zhang, Qing Yang, Minjing Li, Xun Hou, and Feng Chen**

The compact and lightweight infrared (IR) optics devices are highly demanded in booming applications. However, fabrication of IR optics devices with high efficiency is still technically challenging, especially artificial compound eyes (ACE) with low aberration imaging and large field of view. In this work, a method of femtosecond laser wet etching combining with the "two-step" precision glass molding based on chalcogenide glass is proposed to fabricate glass IR ACE. The as-prepared consists of 6000 ommatidia (diameter of 88 μm and the sag height of 11 μm) arranged in a hexagonal manner with perfect parabolic morphology and high uniformity. The chalcogenide glass IR ACE exhibits excellent optical performance both in IR active imaging and IR passive imaging with high transmittance (60–70%) ranging from 2.5 to 15 μm. The ommatidia have a high resolution up to 20.16 lp mm^{-1}, and imaging with large field of view up to 60° and low aberration can be achieved. Furthermore, the proposed technology shows advantages to fabricate glass IR ACE with low cost and high efficiency, and glass IR ACE shows great potential in IR imaging, robot vision, IR 3D motion tracking, and so on.

1. Introduction

Nature invented the most sophisticated optical imaging system called compound eyes. Composed of thousands of ommatidia spherically distributed over the animal's head, the nature compound eyes possess unique image-sensing characteristics such as low aberration, a wide field of view (FOV), and high-sensitivity detection.[1–3] Those animals with compound eyes are able to perceive their environment and take a swift evasive action when their enemy is approaching.

S. Wang, X. Hou, F. Chen
State Key Laboratory for Manufacturing System Engineering
and Shaanxi Key Laboratory of Photonics Technology for Information
School of Electronic Science and Engineering
Xi'an Jiaotong University
Xi'an 710049, P. R. China
E-mail: chenfeng@mail.xjtu.edu.cn

Q. Yang, M. Li
School of Mechanical Engineering
Xi'an Jiaotong University
Xi'an 710049, P. R. China

F. Zhang
School of Physics Science and Information Technology
Liaocheng University
Liaocheng 252000, P. R. China

The ORCID identification number(s) for the author(s) of this article can be found under https://doi.org/10.1002/admt.202200741.

DOI: 10.1002/admt.202200741

Inspired by the nature compound eyes, many researchers began to imitate biology and create artificial compound eyes (ACE).[4] Many ACE devices have been reported, but most of them can only work in the visible wavelengths,[5–14] which limits the application of ACE devices in the IR bands. Since infrared technology has the advantages of passive work, all day and less susceptible to interference and IR ACE can provide information that most of time cannot be accessed through visible one, it is of great significance to fabricate IR ACE imaging component applied in infrared bands.[15] Besides, compared with polymer materials, ACE made of glass material has the advantages of higher damage threshold, wider response wavelength range, stable chemical properties, and high mechanical strength.[6] Therefore, the fabrication of glass-based ACE will better meet the requirements to work functionally under complex conditions such as high-power laser environments, high temperature and high pressure, dark night, fog, and smoke.

Chalcogenide glasses contain three elements S, Se, Te, and other metal elements, both of which can be easily tailored by glass composition to change its physical and chemical properties.[16,17] Compared with other infrared materials, chalcogenide glass has a smaller temperature coefficient of refractive index so that it is less affected by defocusing phenomenon caused by heat, and the excellent infrared transmission performance of chalcogenide glass (ranging from 0.5 to 25 μm) can meet the application requirements of multispectral transmission. Precise glass molding is proved to be a feasible way to fabricate infrared optics components due to that chalcogenide glass is an amorphous material with low softening temperature.[18] Therefore, chalcogenide glass becomes an attractive material for fabricating infrared optical devices. 3D microfabrication technology based on femtosecond laser has broad application prospects in the field of high-precision free-form surface micro-optics fabrication in recent years.[19–30] Templates with high precision and good morphology on hard materials can be fabricated to realize mass production of micro-optical components. Herein, the method of combining femtosecond laser wet etching technology with "two-step" thermal precision glass molding of chalcogenide glass is proposed for rapid fabrication of glass IR ACE. We demonstrated that glass IR ACE with nearly 6000 ommatidia was fabricated. The ACE morphology was also

characterized by scanning electronic microscope and confocal laser scanning microscope. The high optical performance of the glass IR ACE was investigated by infrared optical microscope, including optical focusing, active and passive imaging, and wide FOV with low aberration. Furthermore, IR ACE was also verified to track the motion of 3D object. All these results have shown the broad prospects for IR imaging with large field of view, IR thermal imaging, and 3D motion detection.[31,32]

2. Results and Discussion

2.1. Fabrication of Chalcogenide Glass IR ACE

In this experiment, femtosecond laser wet etching technology was used to fabricate precise K9 glass ACE templates, as shown in **Figure 1**a. First, femtosecond laser modification. The laser source used in the experiment was 800 nm wavelength at the repetition rate of 1 kHz with the pulse duration at 50 fs. The laser beam was focused on the K9 planoconcave glass surface by an objective lens (NA = 0.45), and ablated thousands of craters with a hexagonal arrangement and a spacing of 90 μm in the manner of point-by-point. The laser power is 17 mW and the laser irradiation time of each crater is 500 ms. Second, hydrofluoric acid (HF) wet etching process. The ablated K9 planoconcave glass was treated with 8% (v/v) HF in ultrasonic water bath for 3 h. Due to the nonlinear effect in the interaction of femtosecond laser with the K9 glass, the so-called Lewis base was generated with greatly enhanced chemical activity in reactions with acids. Therefore, the etching rate of HF to the laser-modified area is higher than that of the nonmodified area during the etching process, and with the progressing of reaction, the rough crater becomes a microconcave lens array with a smooth surface.[5] Then, after the etched K9 planoconcave glass was ultrasonically cleaned in deionized water to remove the impurities and HF acid residues, the ACE template made of K9 glass was fabricated.

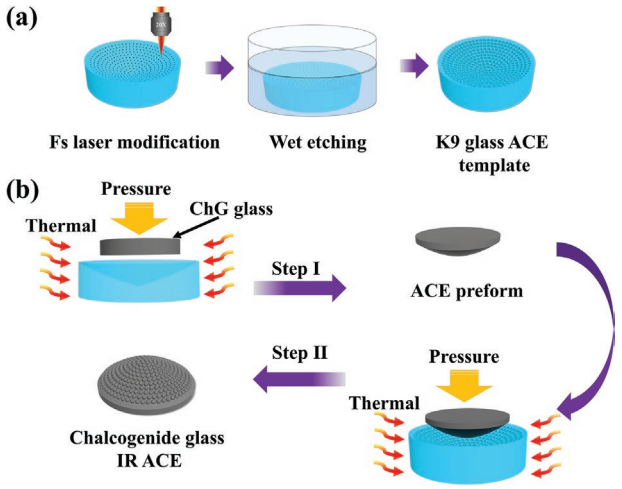

Figure 1. The process to fabricate chalcogenide glass IR ACE. a) The schematic diagram of fabrication of K9 glass ACE template by femtosecond laser wet etching. b) The schematic diagram of fabrication of chalcogenide glass ACE by "two-step" precision glass molding.

The precision glass molding which can realize the replication of micro- and nanostructures with high efficiency and low cost is one of the most promising technologies with which to manufacture chalcogenide glass.[33–35] A "two-step" thermal precision molding process for chalcogenide glass is proposed to fabricate glass IR ACE, which could improve the yield of ACE and avoid large-area microlens of compound eyes template that cannot be transferred in the way of direct imprinting.

Figure 1b depicts the "two-step" thermal precision molding process for chalcogenide glass. The first step is to use the precision glass molding to fabricate the ACE preform. The chalcogenide glass disk ($Ge_{20}Sb_{15}Se_{65}$, diameter is 15 mm and thickness is 3 mm) is vertically placed at the center of K9 planoconcave lens. The entire molding process is carried out in a commercial high temperature furnace. The molding pressure is set to 142 kPa throughout the whole molding process and the molding temperature is set to 370–380 °C for 30 min. The preform can be obtained after subsequent slowly cooling and rapidly cooling. The second step is to place vertically the preform at the center of K9 glass ACE template, and perform the precision molding process again to fabricate the infrared glass ACE with the same molding process as in the first step. The X-ray diffraction (D8 Advance A25, Bruker Corporation, Karlsruhe, Germany) patterns of chalcogenide glass (ChG) both before and after molding are shown in Figure S1 of the Supporting Information. The additional peaks induced by the crystal were not found in the glass after the precision glass molding technology, which indicating that the ChG glass is stable at the corresponding molding condition.[33] By using the "two-step" glass precision glass molding process on the ChG substrate, glass IR ACE was successfully fabricated with 6000 ommatidia.

2.2. The Optical Properties

In order to better characterize the surface morphology, the SEM images of IR ACE were taken. **Figure 2**a–c shows the IR ACE at different high magnification. We can clearly observe that each lens arranged in the way of hexagonal pattern is uniformly distributed on the dome with the spacing of 90 μm and that no obvious shape deformation can be found. These fine microlens structures shown in Figure 2b ensure the excellent optical performance and glass compound eyes with high-quality can be fabricated through our proposed technology in a way of high efficiency and low cost. Five different areas shown in Figure 2c were also chosen for quantitative analysis of ommatidia, which would be discussed later. Such a dimension and an alignment pattern of the microlenses are comparable to the ommatidia of natural compound eyes, showing great potential in developing inspired compound eyes devices.[20]

Furthermore, we observe the 3D morphology of several microlenses on the side part of the IR ACE by a laser confocal scanning microscope (LCSM, OLS4000, Olympus Corporation, Tokyo, Japan), shown in **Figure 3**a. The cross-sectional profile of the microlenses at the side of IR ACE was shown in Figure 3b. We can clearly see the curved outline of the ACE structure, and it is precisely because each microlens is distributed on such an arc-shaped structure that the compound eye has the advantage of imaging with large field of view. We also characterized the

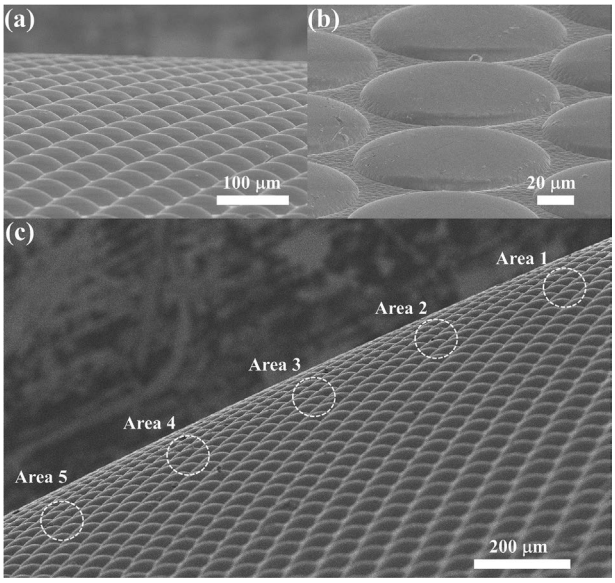

Figure 2. Surface morphology of chalcogenide glass IR ACE. a–c) SEM images of glass IR ACE at different high magnification.

structure of the compound eye at different locations using an optical microscope with an entire height range of 140 μm, and the results are shown in Figure S2 of the Supporting Information. In addition, as shown in Figure 3c, five different areas of the ommatidia on the ACE structure were equally selected, and the diameter and the sag height of those ommatidia were statistically analyzed (Figure 3c). These results reveal that the diameter and the sag height of different areas do not change much and that the microlens array has high fidelity. Transmittance is an important parameter and key feature of optical devices in practical applications. The transmittance of the glass IR ACE is measured by Fourier infrared spectrometer (Nicolet iS 10, Thermo Fisher, Waltham, MA, USA). The result shown in Figure 3d reveals that glass IR ACE has high transmittance with a wavelength ranging from 2.5 to 15 μm and indicates a huge application prospect in IR application.

2.3. Imaging Test

The imaging performance of the IR ACE was tested and the experiment setup is shown in **Figure 4**a. The whole experiment setup includes the broad spectrum light source, a 3D translation stage, an IR objective lens (Plan Apo, Nikon, Tokyo, Japan), and an IR charge-coupled device (CCD) camera (OW 1.7-CL-320, Raptor photonics, Northern Ireland, England) with the sensitive wavelength ranging from 0.4 to 1.7 μm. In the experiment, a black sheet with a letter F patterned on was placed between broad spectrum light source and IR ACE, and the distance between the object and the IR ACE can be adjusted via 3D translation stage. Figure 4b–e shows the letter F clearly imaged at different focal distances by microlenses integrated with an IR objective lens (20×/NA = 0.4) from the lower left corner of the field of view to the upper right corner. Besides, Video S1 of the Supporting Information is also taken to show the clear image by microlens. From that video we can observe that as the distance between the IR objective lens (20×/NA = 0.4) and the ACE is gradually increased, the image of letter "F" also changes from blurred to clear and back to blurred again, which indicates the 3D curved focal plane of ACE.

To quantitatively analyze the imaging quality of compound eyes, a standard USAF1951 resolution test chart is used to characteristic the resolution of ACE. **Figure 5**a shows the imaging

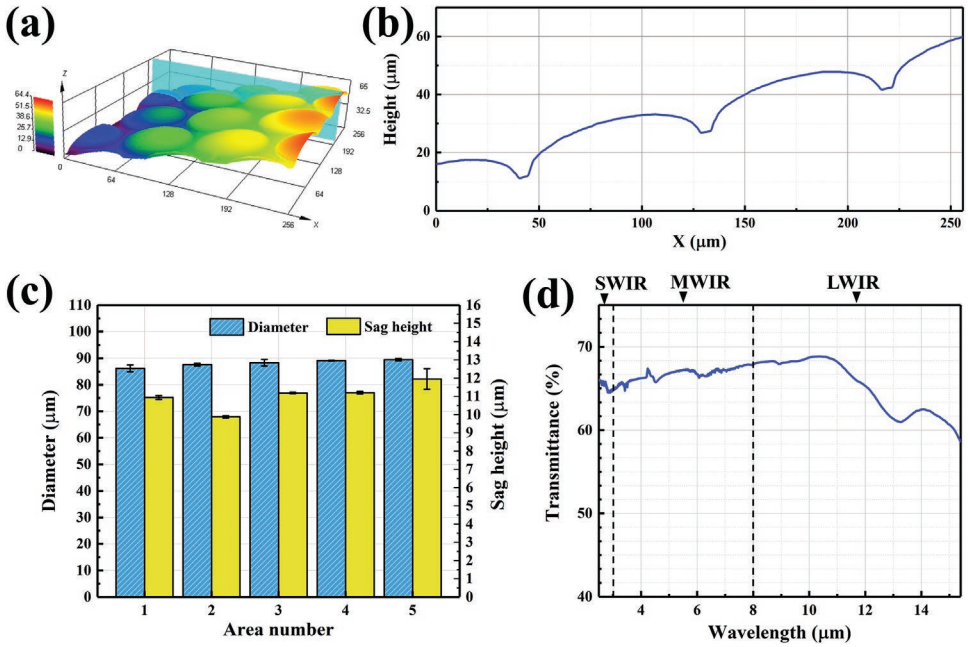

Figure 3. a) The 3D morphology of the side portion of glass IR ACE measured by laser confocal scanning microscope (LCSM). b) The cross-section of the side portion of glass IR ACE. c) The measured diameters and sag heights of ommatidia located at different areas. d) The measured transmittance of the glass IR ACE.

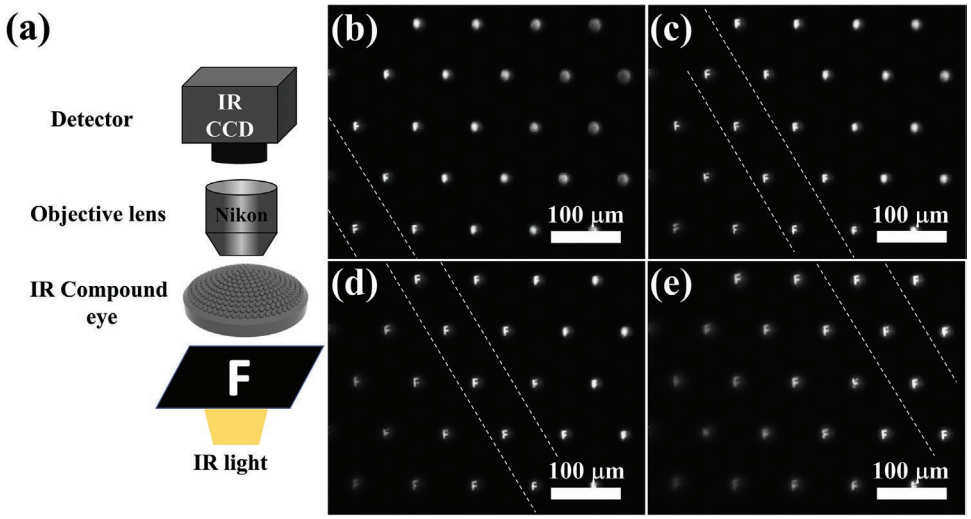

Figure 4. a) The IR imaging experiment setup. b–e) The IR active imaging of a black sheet with letter "F" printed on at different focal distances.

result of the microlens located at the top of the ACE dome on the resolution test chart, from which group 4, element 3 can be distinguished very well, indicating that the resolution of 20.16 lp mm^{-1}. The IR passive imaging performance of ACE is also characterized by using tungsten filament lamp beads as the imaging object. The filament is imaged by ACE integrated with objective lens (50×/NA = 0.42), as shown in Figure 5b. Any object with the temperature above absolute zero emits IR rays and the emitted IR radiation from the object carries specific information. In the case of power-on, the tungsten filament lamp beads heat up, and the filament radiates the IR rays.[15] From Figure 5b, the spiral filament shape can be clearly recognized, which shows great potential of IR ACE in IR passive imaging.

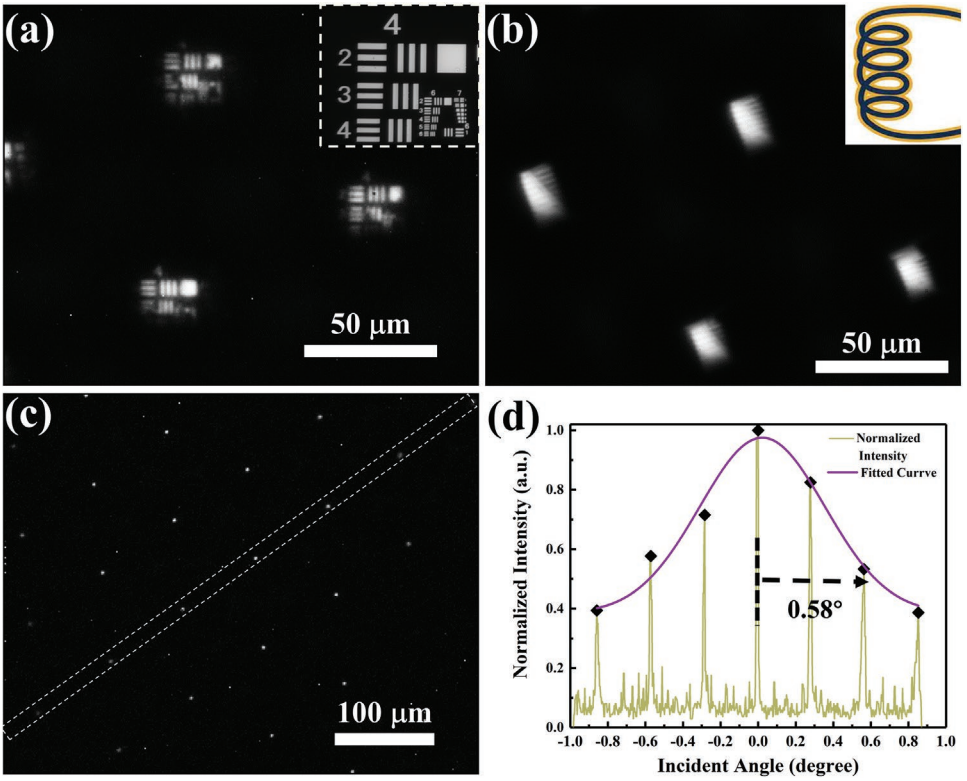

Figure 5. a) The imaging of the USAF1951 resolution test chart by ommatidium of the glass IR ACE and the inset is the USAF1951 resolution test chart. b) The IR passive imaging of the heated tungsten lamp filament magnified when power on and the inset is the IR image of a tungsten lamp filament. c) The foci array distribution of the IR light. d) The measured ASF of the glass IR ACE. The normalized intensities were extracted from the ommatidia selected by the rectangular dotted line box.

In the experiment, we measure the light intensity of foci array to evaluate uniformity of each lens located at the center of ACE, and the foci array image is captured by CCD shown in Figure 5c. Since the ACE is not a planar structure, the gray value of each foci array is not equal. The cross-sectional intensity distribution of those foci selected by the rectangular dotted line box is similar to the dome morphology of ACE structure (Figure 5c). Furthermore, the angular sensitivity function (ASF) is also characterized by measuring the peak intensity of each foci array, and the curve fits very well with the Gauss distribution (Figure 5c). From the ASF curve, it can be found that the full width at half-maximum (FWHM) is 1.16°, which indicates that the light intensity received by each ommatidium would decrease to half when the light is incident at the angle of 0.58°. In addition, the FWHM angle is larger than the interommatidial angle (0.27°, calculated by the formula of d/R, where R is the radius of curvature of the dome of ACE and d is the distance between two adjacent ommatidia). It is noted that the optical overlap would occur between adjacent ommatidium, but the self-written waveguides can be introduced to avoid this optical overlap.[6–8]

2.4. IR ACE for Tracking of Objects Motion

Artificial compound eyes combining with the signal receiving and processing system are feature in high spatial and temporal resolution. An experiment setup was designed to illustrate IR ACE potential of moving object detection and get better understanding of how arthropods perceive other creatures such as a moving ant (**Figure 6**a). A moving ant at different moment is imaged by ommatidia at different location from different angles. At the beginning, the head of ant can be clearly seen (Figure 6b), and gradually we can see the ant passing through the entire field of vision and gradually disappear (Figure 6c,d). More detailed information can be obtained from Video S2 of the Supporting Information. Combined with the subsequent signal processing system and image processing algorithm, the position and moving speed of the ants can be obtained.[36] Those results reveal IR ACE has huge potential for IR 3D motion tracking.

2.5. FOV Test

Thousands of ommatidia are closely distributed on the dome morphology, which makes the ACE structure is able to image with large field of view. In the experiment, the collimated continuous wave laser with a wavelength of 1064 nm is irradiated on the compound eye, and the FOV is also measured by observing the foci image magnified with objective lens (20×/NA = 0.45) and captured by IR CCD when rotating the ACE.[7] The ACE is rotated at 0°, 16°, and 30°, respectively, and the corresponding foci images are captured (**Figure 7**a–c). As can be seen from these results, the final experimental FOV is 60°. To further characterize the optical performance of the IR ACE, the 3D point spread function of the IR ACE imaging at different angles was tested. Figure 7d–f demonstrates the test results of the 3D point spread function at 0°, 16°, and 30°, respectively. It can be seen from these results that under different angles, the ACE imaging has almost no serious distortion, which indicates that the fabricated ACE has the characteristics of imaging with large field of view and low aberration.

3. Conclusion

A low-cost and high-efficiency method for fabricating glass-based infrared compound eyes has been proposed. By combining femtosecond laser wet etching technology with "two-step"

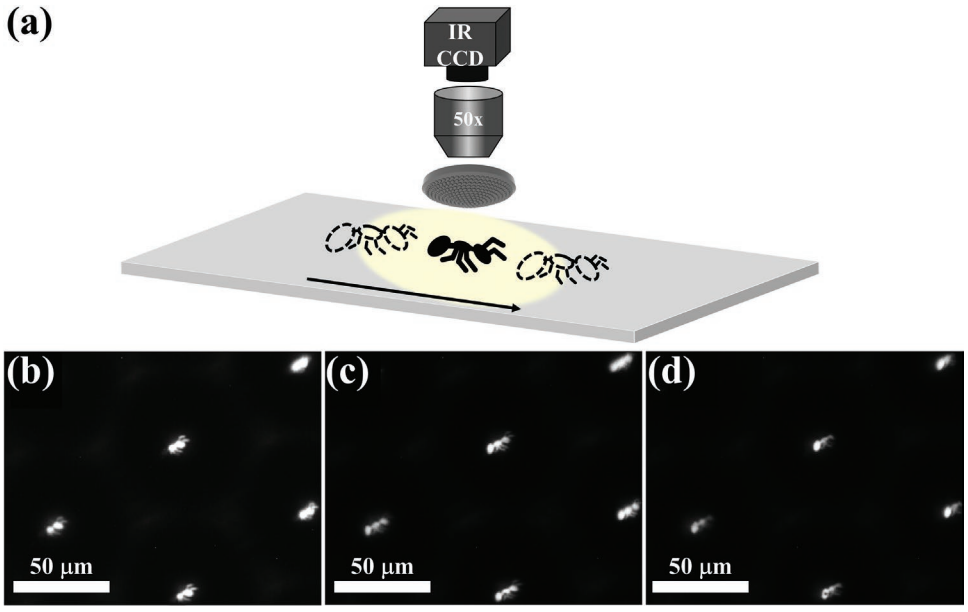

Figure 6. a) Schematic setup for IR ACE to detect the movement of a moving ant. b–d) Different parts of moving ant imaged by IR ACE during the movement.

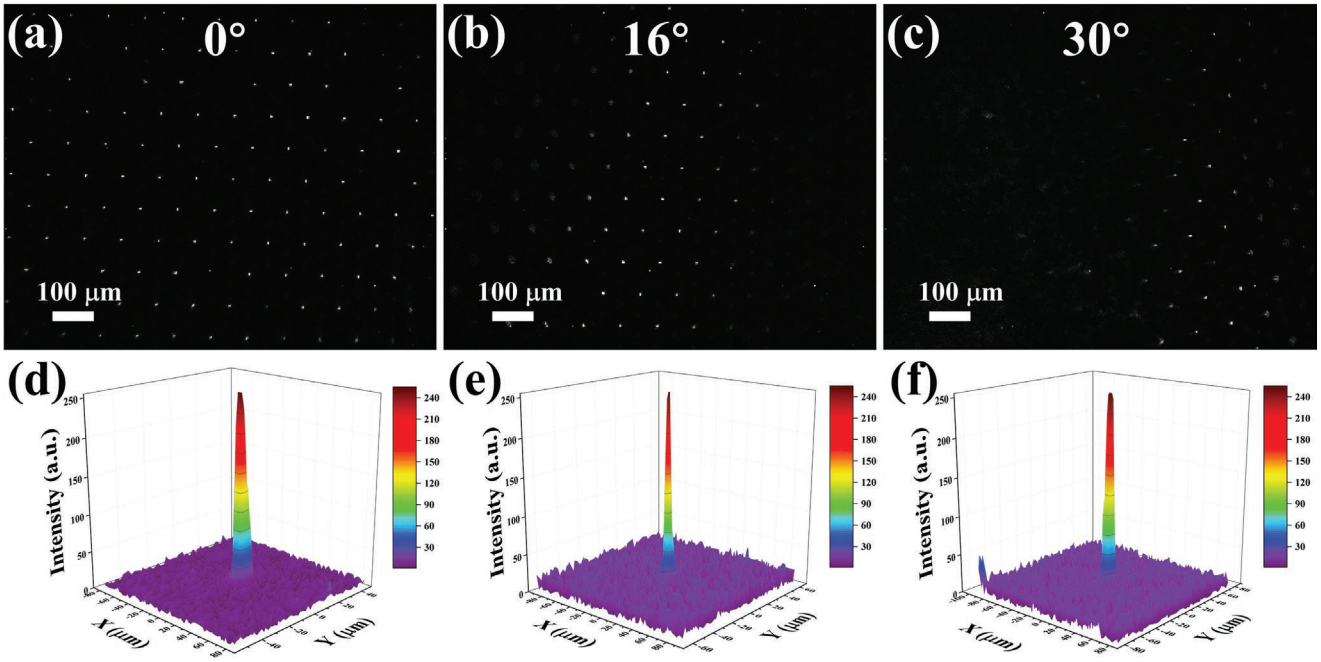

Figure 7. a–c) The images of foci array of the glass IR ACE irradiated by 1064 nm laser with incident angle of 0°, 16°, and 30°, respectively. d–f) The measured PSF of ommatidium when the laser incident at angle of 0°, 16°, and 30°, respectively.

precision chalcogenide glass molding, infrared compound eyes made of chalcogenide glass can be fabricated. Almost 6000 ommatidia arranged in hexagons are distributed on the dome shape with high uniformity. The average diameter of each ommatidium is 88 μm, and the average sag height is 11 μm. The ommatidium also shows great active imaging performance with the high resolution up to 20.16 lp mm^{-1}. After infrared passive imaging test, IR ACE also showed excellent performance in the field of infrared thermal imaging with high transmittance up to 60–70% from 2.5 to 15 μm. Besides, Infrared ACE can achieve imaging with large FOV up to 60° and low aberration. Due to its excellent optical performance and stable physical properties, IR ACE not only can be applied in IR bands, but also can meet the requirements in complex environments such as night environment and strong power lasers, which have great application prospects in IR thermal sensing, robot vision, and night vision with large FOV.

4. Experimental Section

Fabrication of K9 Glass ACE Template: The regeneratively amplified Ti:sapphire laser system (coherent libra-usp-he) generated central wavelength of 800 nm laser with a pulse duration of 50 fs and repetition rate of 1 kHz. The laser was focused by an objective lens (20×/NA = 0.45) on the surface of K9 planoconcave glass. The laser power was set to 17 mW and the irradiation time of each crater was 500 ms. Craters were created with a hexagonal arrangement and a spacing of 90 μm. Then the modified K9 planoconcave glass was immersing in 8% (v/v) HF prepared by diluting commercial 40% (v/v) HF solution with deionized water for 3 h at room temperature.

Fabrication of Chalcogenide Glass IR ACE via "Two-Step" Precision Glass Molding: The first step was to place the chalcogenide glass disk ($Ge_{20}Sb_{15}Se_{65}$, diameter is 15 mm and thickness is 3 mm) vertically at the center of K9 planoconcave lens in a commercial high temperature furnace. The molding pressure was set to 142 kPa throughout the whole molding process and the molding temperature was set to 375 °C for 30 min. The chalcogenide glass disk changed into preform via first step. In the second step, the preform was sandwiched into the K9 glass ACE template and was performed the precision molding process again to fabricate the infrared glass ACE with the same parameters as the first step.

Characterization of Chalcogenide Glass IR ACE Morphology: The surface morphology of IR ACE was measured through scanning electron microscope (Hitachi, FlexSEM 1000) and LCSM (OLS4000, Olympus Corporation, Tokyo, Japan).

Characterization of Chalcogenide Glass IR ACE Optical Performance: The transmittance of chalcogenide glass IR ACE was measured by Fourier infrared spectrometer (Nicolet iS 10, Thermo Fisher, Waltham, MA, USA). The IR imaging performance was measured by IR CCD (OW 1.7-CL-320, Raptor photonics, Northern Ireland, England).

Supporting Information

Supporting Information is available from the Wiley Online Library or from the author.

Acknowledgements

S.W. and F.Z. contributed equally to this work. This work was supported by the National Natural Science Foundation of China under Grant Nos. 12127806, 61875158, and 62175195, the International Joint Research Laboratory for Micro/Nano Manufacturing and Measurement Technologies, and the Fundamental Research Funds for the Central Universities.

Conflict of Interest

The authors declare no conflict of interest.

Data Availability Statement

Research data are not shared.

Keywords

chalcogenide glass, compound eyes, femtosecond laser, infrared, microfabrication

Received: May 6, 2022
Revised: June 20, 2022
Published online:

[1] Y. M. Song, Y. Xie, V. Malyarchuk, J. Xiao, I. Jung, K.-J. Choi, Z. Liu, H. Park, C. Lu, R.-H. Kim, R. Li, K. B. Crozier, Y. Huang, J. A. Rogers, *Nature* **2013**, *497*, 95.
[2] K. H. Jeong, J. Kim, L. P. Lee, *Science* **2006**, *312*, 557.
[3] K. Kim, K. W. Jang, J. K. Ryu, K. H. Jeong, *Light: Sci. Appl.* **2020**, *9*, 28.
[4] L. P. Lee, R. Szema, *Science* **2005**, *310*, 1148.
[5] F. Liu, H. Bian, F. Zhang, Q. Yang, C. Shan, M. J. Li, X. Hou, F. Chen, *Adv. Opt. Mater.* **2020**, *8*, 1901767.
[6] X. Q. Liu, S. N. Yang, L. Yu, Q. D. Chen, Y. L. Zhang, H. B. Sun, *Adv. Funct. Mater.* **2019**, *29*, 1900037.
[7] Z. Deng, F. Chen, Q. Yang, H. Bian, G. Du, J. Yong, C. Shan, X. Hou, *Adv. Funct. Mater.* **2016**, *26*, 1995.
[8] D. Wu, J. N. Wang, L. G. Niu, X. L. Zhang, S. Z. Wu, Q. D. Chen, L. P. Lee, H. B. Sun, *Adv. Opt. Mater.* **2014**, *2*, 751.
[9] J. J. Cao, Z. S. Hou, Z. N. Tian, J. G. Hua, Y. L. Zhang, Q. D. Chen, *ACS Appl. Mater. Interfaces* **2020**, *12*, 10107.
[10] Z. C. Ma, X. Y. Hu, Y. L. Zhang, X. Q. Liu, Z. S. Hou, L. G. Niu, L. Zhu, B. Han, Q. D. Chen, H. B. Sun, *Adv. Funct. Mater.* **2019**, *29*, 1903340.
[11] F. Serra, M. A. Gharbi, Y. M. Luo, I. B. Liu, N. D. Bade, R. D. Kamien, S. Yang, K. J. Stebe, *Adv. Opt. Mater.* **2015**, *3*, 1287.
[12] J. Li, W. J. Wang, X. S. Mei, D. X. Hou, A. F. Pan, B. Liu, J. L. Cui, *ACS Appl. Mater. Interfaces* **2020**, *12*, 8870.
[13] H. W. Liu, F. Chen, Q. Yang, P. B. Qu, S. G. He, X. H. Wang, J. H. Si, X. Hou, *Appl. Phys. Lett.* **2012**, *100*, 133701.
[14] B. S. Zhang, G. Chen, M. M. C. Cheng, J. C. M. Chen, Y. Zhao, *OSA Continuum* **2020**, *3*, 2553.
[15] Q. C. Shen, Z. Luo, S. Ma, P. Tao, C. Y. Song, J. B. Wu, W. Shang, T. Deng, *Adv. Mater.* **2018**, *30*, 1707632.
[16] N. Ostrovsky, D. Yehuda, S. Tzadka, E. Kassis, S. Joseph, M. Schvartzman, *Adv. Opt. Mater.* **2019**, *7*, 1900652.
[17] H. T. Lin, Y. Song, Y. Z. Huang, D. Kita, S. Deckoff-Jones, K. Q. Wang, L. Li, J. Y. Li, H. Y. Zheng, Z. Q. Luo, H. Z. Wang, S. Novak, A. Yadav, C. C. Huang, R. J. Shiue, D. Englund, T. Gu, D. Hewak, K. Richardson, J. Kong, J. J. Hu, *Nat. Photonics* **2017**, *11*, 798.
[18] T. Zhou, Z. Zhu, X. Liu, Z. Liang, X. Wang, *Micromachines* **2018**, *9*, 337.
[19] S. Tong, H. Bian, Q. Yang, F. Chen, Z. Deng, J. Si, X. Hou, *Opt. Express* **2014**, *22*, 29283.
[20] H. Bian, Y. Wei, Q. Yang, F. Chen, F. Zhang, G. Q. Du, J. L. Yong, X. Hou, *Appl. Phys. Lett.* **2016**, *109*, 221109.
[21] M. J. Li, Q. Yang, J. L. Yong, J. Liang, Y. Fang, H. Bian, X. Hou, F. Chen, *Opt. Express* **2019**, *27*, 35903.
[22] H. W. Liu, F. Chen, X. H. Wang, Q. Yang, D. S. Zhang, J. H. Si, X. Hou, *Opt. Commun.* **2009**, *282*, 4119.
[23] F. Chen, Z. F. Deng, Q. Yang, H. Bian, G. Q. Du, J. H. Si, X. Hou, *Opt. Lett.* **2014**, *39*, 606.
[24] D. Z. Tan, Z. Wang, B. B. Xu, J. R. Qiu, *Adv. Photonics* **2021**, *3*, 024002.
[25] D. S. Zhang, F. Chen, G. P. Fang, Q. Yang, D. G. Xie, G. J. Qiao, W. Li, J. H. Si, X. Hou, *J. Micromech. Microeng.* **2010**, *20*, 075029.
[26] J. Yong, Q. Yang, X. Hou, F. Chen, *Ultrafast Sci.* **2022**, *2022*, 9895418.
[27] J. Yong, F. Chen, J. Huo, Y. Fang, Q. Yang, H. Bian, W. Li, Y. Wei, Y. Dai, X. Hou, *ACS Omega* **2018**, *3*, 1395.
[28] J. Yong, F. Chen, Q. Yang, D. Zhang, H. Bian, G. Du, J. Si, X. Meng, X. Hou, *Langmuir* **2013**, *29*, 3274.
[29] J. L. Yong, F. Chen, Y. Fang, J. L. Huo, Q. Yang, J. Z. Zhang, H. Bian, X. Hou, *ACS Appl. Mater. Interfaces* **2017**, *9*, 39863.
[30] Z. Lin, M. Hong, *Ultrafast Sci.* **2021**, *2021*, 9783514.
[31] Kenry, Y. Duan, B. Liu, *Adv. Mater.* **2018**, *30*, 1802394.
[32] C. Y. Shi, Y. Y. Wang, C. Y. Liu, T. S. Wang, H. X. Zhang, W. X. Liao, Z. J. Xu, W. X. Yu, *Opt. Express* **2017**, *25*, 32333.
[33] D. H. Cha, H. J. Kim, Y. Hwang, J. C. Jeong, J. H. Kim, *Appl. Opt.* **2012**, *51*, 5649.
[34] F. Zhang, Q. Yang, H. Bian, M. J. Li, X. Hou, F. Chen, *Materials* **2020**, *13*, 3490.
[35] L. Zhang, L. Y. Zhou, W. C. Zhou, S. Q. Zhang, A. Y. Yi, *Precis. Eng.* **2020**, *66*, 87.
[36] X. J. Hu, J. M. Zhu, Q. H. Hu, J. J. Zheng, D. Y. Yang, F. L. Zhou, Y. X. Cheng, Y. Yang, *Biosens. Bioelectron.* **2022**, *195*, 113670.